NAP-XPS Probes the Electronic Structure of the Mg–Al–Cl Layered Double Hydroxide upon Controlled Hydration

Romain Coustel, Anthony Boucly, Erwan André, Arnaud Di Bitetto, Fabrice Bournel, Jean-Jacques Gallet, François Rochet, Cédric Carteret

▶ **To cite this version:**

Romain Coustel, Anthony Boucly, Erwan André, Arnaud Di Bitetto, Fabrice Bournel, et al.. NAP-XPS Probes the Electronic Structure of the Mg–Al–Cl Layered Double Hydroxide upon Controlled Hydration. Journal of Physical Chemistry C, 2023, 127 (8), pp.4144-4153. 10.1021/acs.jpcc.2c05362 . hal-04029492

HAL Id: hal-04029492
https://hal.science/hal-04029492

Submitted on 15 Mar 2023

HAL is a multi-disciplinary open access archive for the deposit and dissemination of scientific research documents, whether they are published or not. The documents may come from teaching and research institutions in France or abroad, or from public or private research centers.

L'archive ouverte pluridisciplinaire **HAL**, est destinée au dépôt et à la diffusion de documents scientifiques de niveau recherche, publiés ou non, émanant des établissements d'enseignement et de recherche français ou étrangers, des laboratoires publics ou privés.

NAP-XPS probes the electronic structure of the Mg-Al-Cl layered double hydroxide upon controlled hydration

Romain Coustel[1], Anthony Boucly[2], Erwan André[1], Arnaud Di Bitetto[1], Fabrice Bournel[2,3], Jean-Jacques Gallet[2,3], François Rochet[2], Cédric Carteret[1]*

1 Université de Lorraine, CNRS, LCPME, F-54000 Nancy, France.

2 Sorbonne Université, CNRS (UMR 7614), Laboratoire de Chimie Physique Matière et Rayonnement, 4 place Jussieu, 75252 Paris Cedex 05, France.

3 Synchrotron SOLEIL, L'Orme des Merisiers, Saint-Aubin, BP 48, F-91192, Gif-sur-Yvette, France.

KEYWORDS: LDH, NAP-XPS, hydration, electronic structure, radiolysis

ABSTRACT

The hydration of $[Mg_2Al(OH)_6]^+[Cl^-, y\ H_2O]$ LDH was investigated by volumetric water adsorption, X-ray diffraction, Fourier Transformed Infrared (FTIR) and Near Ambient Pressure X-ray Photoelectron (NAP-XPS) spectroscopies. It was demonstrated that water uptake into interlayer region can be quantify by NAP-XPS. The LDH's electronic structure is assessed for increasing relative humidity (*RH*) up to 0.044. Cl 2p level appears essentially unaffected by water uptake but, as supported by DFT calculation, H-bonds between chloride and water induce Cl 3p orbitals splitting. At *RH* = 0.7, LDH is covered by a water film that contains Mg and Cl species but no Al. Soft X-ray radiolysis of hydrated Cl species induces the formation of oxidized Cl species.

TEXT

Introduction

Water is ubiquitous on Earth and then takes part in many chemical, physical or biological processes. Materials interactions with water is therefore an issue of primary importance to control their properties and their fate in environmental conditions. X-ray Photoelectron Spectroscopy (XPS) is a tool of choice to probe the electronic structure in material science. Nevertheless, because of the low electron mean free path in the gas phase, XPS analysis has been limited to the study of materials under Ultra High Vacuum (UHV). The last generation of XPS spectrometers allows to go beyond this pressure limitation. Indeed, it is now possible to maintain the electron analyzer under UHV while the sample is exposed to pressures of the order of a few mbar, *i.e.* Near Ambient Pressure (NAP). NAP-XPS offered new opportunities in the field of heterogenous catalysis (gas/solid interface)[1,2] and made also possible to probe gas/liquid interface, *e.g.* the study of solution surfaces began a decade ago.[3,4] Recently, the behavior of swelling clays whose layered structure allows the adsorption of a large amount of water was examined too.[5] Among lamellar materials, double lamellar hydroxides (LDH) has been widely studied as fire retardant,[6] catalyst,[7,8] drug releaser,[9] pollutants adsorbant,[10,11] or antibacterial agent[12]. LDH properties depend on their hydration state which is the subject of a thriving research field.[10,13,14] Nevertheless, as far as we know, their electronic structure in hydrated state has not already been examined by NAP-XPS, which is the point of this work.

LDHs are a class of natural and synthetic materials with brucitic sheets made of di (M^{II}: Mg^{2+}, Fe^{2+}, Ni^{2+}, ...) and tri-valent (M^{III}: Al^{3+}, Fe^{3+}, ...) hydroxide octahedra. These positively charged sheets are separated by hydrated anions (A^{n-}: Cl^-, SO_4^{2-}, NO_3^-, ...). Their general chemical formula

is: $[M^{II}_{1-x}M^{III}_{x}(OH)_2]^{x+}[(A^{n-})_{x/n},y\ H_2O]$ where the layer charge density (x) ranges between 0.20 and 0.33 for most of the cationic couples. In this work, an archetypal LDH with formula $[Mg_2Al(OH)_6]^{+}[Cl^{-},\ y\ H_2O]$ (labelled MgAl-Cl-LDH) has been chosen. This material has been characterized by water adsorption volumetry, X-ray diffraction (XRD) and Fourier Transformed Infra-Red (FTIR) spectroscopy under vacuum and ambient conditions. Its electronic structure under different hydration conditions has been probed by NAP-XPS. DFT simulations have also been carried out to rationalize experimental results.

It is noteworthy that X-ray induces water (or hydrated species) radiolysis.[5,15–17] In this regard, we previously reported the radiolysis of an organic molecule (pyridine) inserted in the interlayer of a hydrated smectite[5]. The radiolysis of water in contact with oxides is largely determined by the reactivity of electron hole pairs produced in the oxide[18]. Studying LDH offers the opportunity to work on materials made of positively charged oxide lamellae with anions as intercalated counterions, while smectite clays are negatively charged layers with intercalated cations. This could possibly impact the selection of the reacting particle attracted in the interlayer (electron: reduction, hole: oxidation). At high relative humidity (*RH*), LDH is covered by a film that contains hydrated Mg and Cl species. This situation is rather similar to the case of alkali halide brines studied by Tissot *et al.*[3,4], and it can be compared to the classical studies on radiolysis in water, since the contribution of the solid oxide is absent. Therefore, the comparison with the low *RH* solid LDH case will be of great interest.

Methods

The $[Mg_2Al(OH)_6]^+[Cl^-, y\ H_2O]$ LDH was prepared as previously described.[10,19] Coprecipitation at low supersaturation was performed by slow addition (0.3 mL min^{-1}) of 200 mL of solution containing 0.4 mol L^{-1} of $Mg^{II}Cl_2$ and $Al^{III}Cl_3$ (Mg/Al = 2) into 200 mL of basic solution containing 0.25 mol L^{-1} of Na_2CO_3. The pH was kept constant at 11 by simultaneous addition of NaOH (1 mol L^{-1}) solution using an automatic titrator device (736 GP Titrino, Metrohm). The mixture obtained was divided by 4, and each fraction underwent a hydrothermal treatment at 100 °C for 20 h (in a recipient of 100 mL) and was then centrifuged and washed 3 times with deionized water. Solids were finally dried in air at room temperature for 24 h. Carbonate to chloride exchange was carried out by dispersion of 0.662 mmol of carbonate-containing LDH in 50 mL of ethanol.[10,19,20] Then 81 µL of 37% HCl was added, and exchange was performed under nitrogen flow, with vigorous stirring for 1 h at 50 °C. The materials obtained were centrifuged and washed with ethanol once and dried in air at 50 °C for 15 h. In the following, the LDH sample was labeled MgAl-Cl-LDH for the sake of simplicity.

Water vapor adsorption–desorption isotherms at 298 K were obtained using a MicrotracBEL Belsorp-Max volumetric adsorption analyzer equipped with three pressure sensors (1.33 bar, 13.3 mbar, and 0.133 mbar). A long acquisition time (3 days per isotherm) was required because of the slow equilibrium kinetics. Investigated sample was outgassed under vacuum (residual pressure of 3×10^{-6} Pa). Volumetric measurements were normalized considering the molar mass of water free MgAl-Cl-LDH ($M([Mg_2Al(OH)_6]^+[Cl^-])$ = 213,1 g mol^{-1}) in order to derive the number of adsorbed water compound per chloride ion for increasing relative humidity ($RH = P/P_{sat}$(298 K), with P the water pressure and P_{sat} = 31 mbar the saturation water pressure at 298 K).

XRD was performed by using a Panalytical X'Pert Pro diffractometer and an X'Celerator as a detector. Data collections were carried out using 0.02 rad Soller slits, programmable divergence and antiscatter slits. The XRD patterns were recorded using the monochromatized $K\alpha_1$ line (λ= 1.5406 Å) using a Cu anode X-ray tube and a Ge(111) monochromator. Measurements were performed at room temperature in ambient condition (*RH* ~ 0.3) or under secondary vacuum (10^{-5} mbar) using a TTK450 cell from Anton Paar.

Infrared studies were performed on an FT-IR spectrometer Thermo Nicolet 8700 with a DTGS detector and KBr beamsplitter. The spectral resolution was 4 cm^{-1} and the acquisition time was 1 minute. Samples were pellets made of a ground mixture of dried KBr (FTIR grade) and 1% weight of LDH powder pressed up to 5 tons. A pure KBr pellet was used as background. Measurements were performed at room temperature in ambient condition (*RH* ~ 0.3) or under secondary vacuum (10^{-5} mbar).

X-ray photoelectron spectra under Ultra High Vacuum (UHV) were recorded with a hemispherical analyzer (KRATOS Axis Ultra), fitted with a DLD detection. The pass energy was 20 V. The source was a monochromatized Al K_α line ($h\nu$ = 1486.6 eV) with a spot size of 0.7 mm × 0.3 mm). The overall energy resolution, resulting from monochromator and electron analyzer bandwidths, leads to *FWHM(*Ag $3d_{5/2}$) better than 800 meV on Ag^0. Photoelectrons were detected at an angle normal to the sample surface.

As LDH is an insulating material, differential charging was eliminated using a flood gun. NAP-XPS measurements were performed at TEMPO beamline of synchrotron SOLEIL with a station built by SPECS (Phoibos 150-NAP electron analyzer). Details on the TEMPO beamline can be found elsewhere.[21] The beamline and the analyzer are protected from the high pressure (<20 mbar)

of the analysis chamber by differential pumping. The sample holder is mounted on a vertical manipulator, and the analyzer axis is perpendicular to the sample surface. The windowless beam entrance axis makes an angle of 54° with the analyzer axis, while the polarization is horizontal. The sample surface was brought to the NAP-XPS nozzle aperture (of diameter 0.3 mm) at a short distance of ~1 mm to minimize the photoelectron inelastic scattering in the gas phase. Spectra were obtained with photon energy of 420 eV or 1100 eV, a pass-energy of 50 V and a slit of 7 mm × 20 mm, corresponding to an analyzer resolution of 200 meV leading to a total spectral resolution (*i.e.* electron spectrometer and beamline) of 225 meV.

For all XPS spectra, a Shirley background was subtracted from the photoemission peaks. Curve fitting was carried out with sums of Voigt or pseudo-Voigt functions (with a Gaussian percentage of 70 %).

LDH hydration was carried out in the NAP-XPS reaction/analysis chamber. The sample temperature was regulated from 1°C to 20°C using a Peltier cooler. Water vapor (double distilled water (DDW, 18.2 MΩ cm) was purified by about 10 pump-and-thaw cycles) or Ar gas are introduced via leak valves into the analysis/reaction chamber. The chamber is itself pumped out via the differential pumping of the analyzer nozzle and the windowless beamline entrance (for more details see [2]). Varying the opening of the leak valve allows to get the desired pressure. NAP-XPS measurements were performed at least 10 min after the pressure steady state is reached. According to volumetric adsorption results (not shown) this delay time is sufficient for the samples to be in thermodynamic equilibrium with the gaseous water.

MgAl-Cl-LDH was deposited from water suspension on a gold coated silicon substrate. Because of their low electrical conductivity, LDH under UHV charge positively under X-ray photon

irradiation: the Mg 2p peak appears at ~58 eV binding energy (hv = 1100 eV) while a position of 50 eV is expected. A flood gun cannot be used in NAP conditions. However, the irradiation of the gas phase above the sample leads to the ionization of the gas and hence provides electrons that contribute to compensate for the surface charge. In the absence of water (RH = 0), argon was also used to mitigate sample charging. According to the procedure detailed in [5], the gold substrate was biased positively (+30 V) with respect to the analyzer in order to attract more efficiently negatively charged species, and hence reduce charging more efficiently. Actually, for the LDH (substrate at +30 V, hv = 1100 eV), the apparent binding energy of the Mg 2p component equals 56 eV ($FWHM$ = 2.8 eV) under UHV, 55 eV under 1 mbar of Ar ($FWHM$ = 2.2 eV) and 50.3-50.9 eV ($FWHM$ = 1.7 eV) under water pressures in the range 0.1-4.5 mbar. As charge effect remains substantial at RH = 0.000 (UHV or 1 mbar Ar) when using the NAP-XPS facility, complementary photoemission spectra were also recorded using the conventional KRATOS UHV XPS apparatus fitted under electron bombardment with the flood gun. In all cases, the photoemission spectra were referenced using the Mg 2p core-level binding set at 50.0 eV (as justified in section "results").

One should also note that biasing the sample positively washes out the gas phase core levels contribution in the NAP-XPS spectra.[5] NAP-XPS measurements were performed on MgAl-Cl-LDH sample at 293 K under 1 mbar of Ar and 0.1, 0.3, 0.6 or 1 mbar of water (RH = 0.000, 0.004, 0.013, 0.026 or 0.044, respectively; $P_{sat}(293\ K)$ = 23 mbar). Finally, measurements were performed at high RH = 0.7 (274 K and 4.5 mbar of water, $P_{sat}(274\ K)$ = 6.4 mbar).

DFT calculations were performed with the CRYSTAL14 periodic *ab initio* code.[22,23] The construction of the model structure for MgAl-Cl-LDH has been detailed elsewhere[24–26], and will be briefly summarized hereafter. All calculations have been done on a $(a\sqrt{3} \times 3a \times c)$ supercell (with a and c referring to the intermetallic and interlayer distance respectively), which corresponds

to the monoclinic cell described by Jayanthi *et al.* for Mg-Al-CO_3.[27] Gaussian type 3ζ basis set and the B3LYP-D* functional were used. That functional is based on B3LYP,[28,29] with the addition, through the Grimme approach,[30,31] of a semi-empirical correction for the dispersive forces. Indeed, those forces are expected to play an important role in the layer/layer interactions. The truncation criteria for the bielectronic integrals have been set to 7 7 7 8 18, the threshold on the SCF energy was set to 10^{-10} Ha, a shrinking factor of 4 has been set along the 3 lattice vectors.

Results

1) Volumetric water adsorption

Water adsorption isotherms performed on MgAl-Cl-LDH are shown in Figure 1. Isotherms were acquired with or without pre-annealing treatment (1200 min at 100°C under secondary vacuum). Both isotherms look similar, indicating that no heat treatment is necessary to remove water compound from the interlayer region under secondary vacuum. This result confirms that XPS measurements performed under UHV probe water free MgAl-Cl-LDH. Water uptake reaches 1 water molecule per chloride at 3 % of *RH* and the hysteresis loop extends from *RH* = 3 % up to saturation. Therefore, the interlayer space (*i.e.* microporosity) can accommodate 1.0-1.5 water molecule per chloride while further adsorption may be roughly attributed to capillary condensation and intercrystallite space (*i.e.* mesoporosity) due to crystallites aggregation.

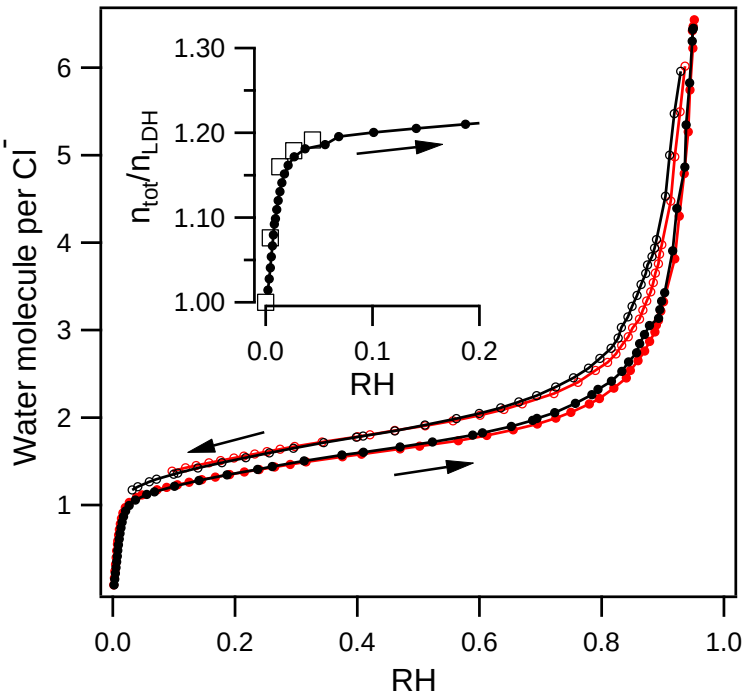

Figure 1. Water vapor adsorption (filled symbol)/desorption (empty symbol) isotherms (298 K) of MgAl-Cl-LDH after annealing (100°C, red) or without annealing (black). n_{tot}/n_{LDH} vs *RH* derived from volumetric (circles) or NAP-XPS measurements (squares) are given in the inset, with n_{tot} and n_{LDH} the amount of oxygen in hydrated and water free MgAl-Cl-LDH, respectively.

2) Structural and vibrational properties

The role of the hydration on the structure of MgAl-Cl-LDH was evaluated by XRD measurement (results not shown). When recorded under secondary vacuum at room temperature, the basal reflections shifted to higher angles evidencing the contraction of the material along the direction perpendicular to the LDH sheet, whereas interatomic distances inside LDH sheet were poorly affected. The interlayer spacing (*d*) declines form 7.69 Å in ambient conditions to 7.44 Å under vacuum, in line with previous report that gave d = 7.45 Å at RH = 0 % and d = 7.70 Å at RH = 10

%.[32]. It should be noted that experimental data agree well with our calculations. DFT simulations predicted *d* equals 7.64 Å for hydrated material (1 water molecule per $[Mg_2Al(OH)_6]^+[Cl^-]$ unit) and 7.37 Å for dehydrated material (see Figure 2).

The vibrational properties of the MgAl-Cl-LDH were probed by FT-IR spectroscopy as function of hydration states (see Figure 2). Bands in the range [300-500 cm^{-1}] remained poorly affected by changing from ambient to vacuum conditions. These bands are attributed to vibration modes of metal-oxygen bonds[33] that then appears essentially unaffected by hydration. OH bending bands [500-1000 cm^{-1}] were remarkably broadened in ambient condition due to the formation of hydrogen bonds between water molecules and LDH hydroxides.

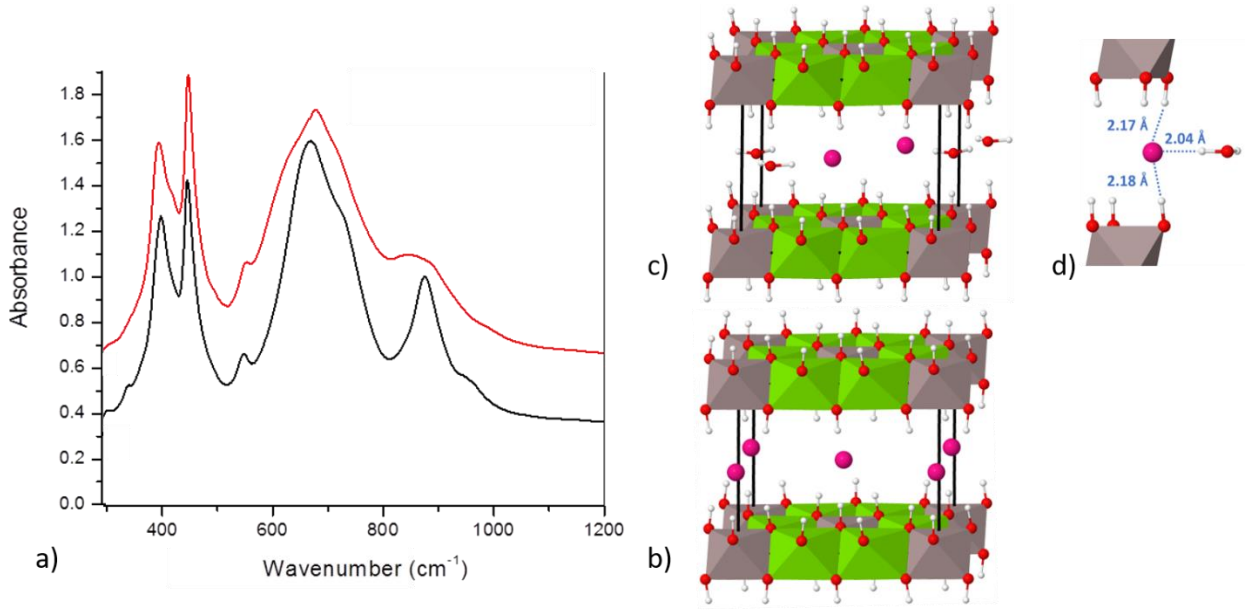

Figure 2. a) FTIR spectra of MgAl-Cl-LDH recorded in ambient conditions (hydrated, red line) and under secondary vacuum (dehydrated, black line) at RT. Calculated structure of MgAl-Cl-LDH: b) dehydrated structure and c-d) hydrated structure (1 water molecule per $[Mg_2Al(OH)_6]^+[Cl^-]$ unit).

3) The evolution of MgAl-Cl-LDH electronic structure upon hydration

NAP-XPS is a unique tool to probe the electronic structure of samples from UHV to conditions close to the ambient pressure. In here, we examine the impact of hydration on electronic properties of MgAl-Cl-LDH.

NAP-XPS spectra recorded in the binding energy range 0-100 eV (see Figure 3, hv = 1100 eV) show Cl 3s (~15 eV), O 2s (~24 eV), Mg 2p (~50 eV), Al 2p (~75 eV) and Mg 2s (~89 eV) core-level peaks. Surface contamination giving rise to C 1s feature is discussed in the Supporting Information (SI), see section S1.

In line with FTIR results indicating that metal-oxygen bonds are poorly affected by hydration, no significant relative shift is observed for Al 2p, Mg 2s and Mg 2p features in the *RH* range of 0.000-0.044. Actually, metallic cations cannot establish direct bond with hydration water because they are embedded within hydroxide sheets. Therefore, all photoemission spectra were referenced using the Mg 2p core-level binding set at 50.0 eV.

The O 2s component grows for increasing *RH*. It should be recalled that in order to suppress the gas phase contribution, a +30 V potential was applied to LDH sample holder with respect to analyzer entrance during NAP-XPS measurements.[5] Therefore, the O 2s enhancement arises only from the water uptake in the solid phase, *i.e.* water insertion into the interlayer region. The evolution of the oxygen content can be assessed from photoemission measurements according to:

$$n_{tot}/n_{LDH} = (A_{O2s}/A_{Mg2p})_{hydrated\ LDH}/(A_{O2s}/A_{Mg2p})_{LDH} \quad (1)$$

with n_{tot} (n_{LDH}) the amount of oxygen in hydrated (water free, respectively) MgAl-Cl-LDH and A_i the photoemission peak area of level *i*. Equation 1 considers that (i) the Mg amount remains

unchanged during hydration and (ii) that O 2s and Mg 2p photoelectrons have nearly equal inelastic mean free paths in the gas phase because their kinetic energies are close (in the range 1000-1100 eV). Then, the use of A_{O2s}/A_{Mg2p} allows getting rid of the photoelectron attenuation by the gas phase.

Results of both photoemission and volumetric adsorption experiments are in fair agreement in the range of *RH* 0.000-0.044 (see inset Figure 1). It comes that NAP-XPS could be used for quantitative evaluation of water adsorption into layered materials. Nevertheless, for higher *RH* (0.219) there is a clear discrepancy between n_{tot}/n_{LDH} values obtained from NAP-XPS (1.45) and volumetric adsorption (1.2). As detailed above, in this *RH* domain, water adsorption leads to the filling of mesopores and to the formation of liquid water multilayers on LDH surface. Due to the short mean free path of the electrons in condensed matter (few nanometers), the condensation of water on LDH surface tends to prevent Mg 2p photoelectrons to escape, leading to an overestimation of the oxygen contribution.

The valence band region photoemission spectrum of dehydrated (*RH* = 0.000) MgAl-Cl-LDH is presented in Figure 3. No feature was identified for a binding energy less than ~2 eV, as expected for an insulator. The valence band spectrum presents an intense peak located at 4.2 eV binding energy as well as poorly structured features up to 13 eV. Density of states obtained by DFT calculations (see Figure 3) shows that the peak at low binding energy corresponds to the Cl 3p states of the Cl^- ion while the component located at higher binding energy presents O 2p character. The computed density of states reported in Figure 3 was rigidly shifted (+4.0 eV on the binding energy scale) to obtain fair agreement between the calculated and experimental valence band features.

For increasing *RH*, the relative intensity of the Cl 3p ($I_{Cl\ 3p}$) component decreases with respect to the features at higher (8 eV) binding energy ($I_{8\ eV}$), *e.g.* $I_{Cl\ 3p} / I_{8\ eV}$ is 2.8, 1.7 or 1.4 for *RH* 0.000, 0.004 or 0.044, respectively. Moreover, at *RH* = 0.044, the Cl 3p peak was shifted to higher binding energy up to 4.5 eV. Both effects resulted from water insertion into the layered material: the water uptake reinforced the O 2p contribution and chloride/water interactions shifted Cl 3p orbitals to higher binding energy. DFT calculations indicate the formation of H-bonds between Cl^- and water molecule (see Figure 2.d), which are lying in the plane that is equidistant from adjacent hydroxyl sheets. Asymmetric hydration leads to the lifting of the degeneracy of the Cl 3p orbitals and the distribution of their energy levels (see the Cl projected density of states in Figure 3).

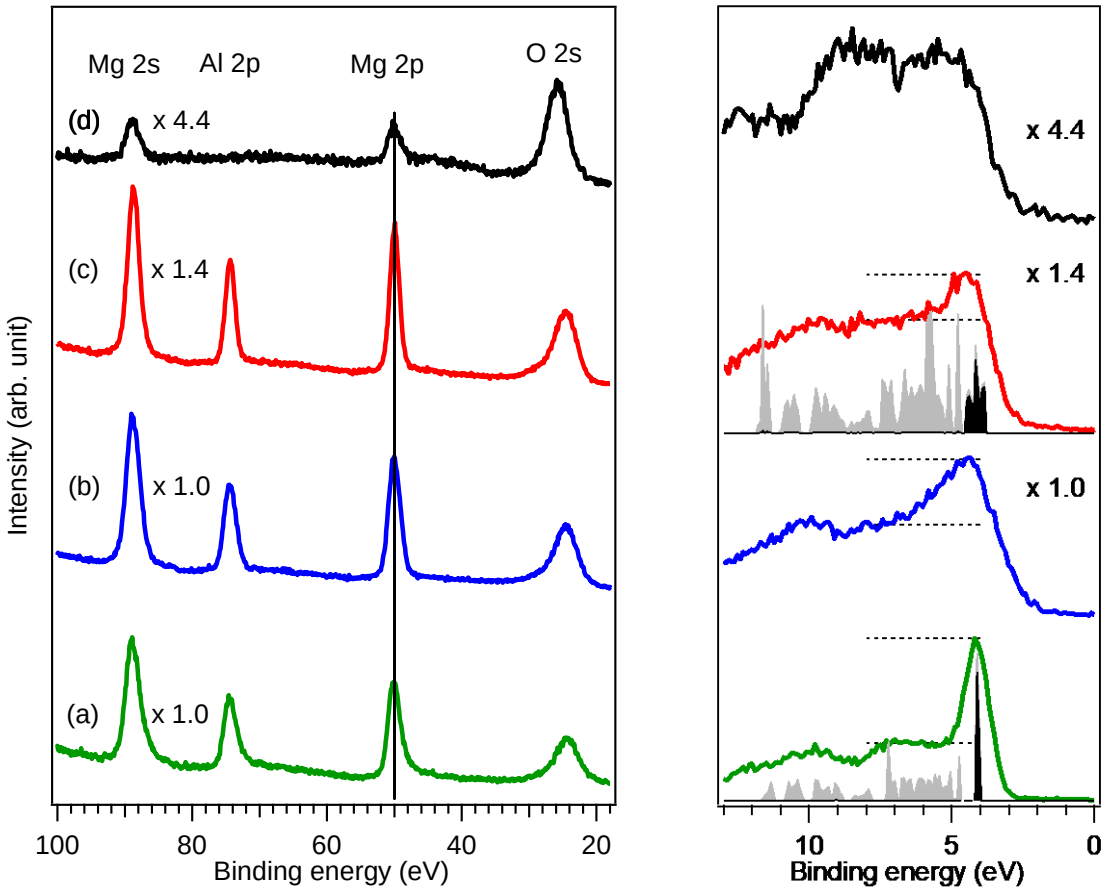

Figure 3. Survey (left) and valence band region (right) XPS spectra of MgAl-Cl-LDH. (a) *RH* = 0.000 (survey: 1 mbar Ar, 293 K, *hv* = 1100 eV; valence band: UHV, 293 K, *hv* = 1487 eV), (b) *RH* = 0.004 (0.1 mbar water, 293 K, *hv* = 1100 eV), (c) *RH* = 0.044 (1 mbar water, 293 K, *hv* = 1100 eV) and (d) Mg-Cl solution *RH* = 0.7 (4.5 mbar water, 274 K, *hv* = 1100 eV). Spectra intensities were normalized to insure proper readability: relative normalization factors are given in the graph for spectra recorded with *hv* = 1100 eV. Calculated (DFT/B3LYP-D/triple-ζ) total (chlorine, respectively) density of states appear as grey (black, respectively) thin line for dehydrated or hydrated (one water compound per chlorine) MgAl-Cl-LDH.

The Cl 2p spectrum of MgAl-Cl-LDH recorded under UHV (see Figure 4) can be fitted by a spin-orbit splitting doublet (Δ = 1.6 eV, with a branching ratio equal to 0.5). The Cl $2p_{3/2}$ component is located at 197.6 eV which corresponds to chloride ion (see Table 1). Spectra obtained for increasing *RH* (up to 0.044) showed broadened components (*FWHM* equal to 1.8 eV at *RH* = 0.044 and 1.1 eV measured under UHV). This symmetric broadening can be ascribed to charging effects that were not fully compensated by sample polarization. For what concerns the asymmetric broadening seen for the water exposed samples, it can be accounted for by a small additional doublet at *ca* + 2 eV above the main doublet. This suggests the formation of Cl species other than the chloride ions. The latter assumption will be discussed further on.

Anyhow, the Cl $2p_{3/2}$ binding energy position due to the Cl^- anions (the main doublet) remained essentially unshifted when hydration takes place. Boucly *et al.*[5] recently reported a NAP-XPS study focusing on the hydration of strontium-hydroxyhectorite, where Sr^{2+} ions compensated the negative charge of the clay layers. When *RH* increases from 0 to 0.07, the binding energy of the Sr $3d_{5/2}$ slightly diminishes by ~0.3 eV. Such chemical shift effect was interpreted in terms of an initial state effect, *i.e.* a change in the electrostatic energy felt by the Sr^{2+} resulting from swelling and/or by final-state effect, *i.e.* a change in the dielectric screening due to Sr^{2+} hydration. In the case of MgAl-Cl-LDH, both initial and final state effects on the Cl 2p level of the interlayer chloride appear weaker or offset one another. However, hydration significantly affects the chloride Cl 3p binding energy that shifts by +0.3 eV with increasing *RH*. This unexpected result reflects the fact that Cl 3p valence electrons are more sensitive to changes in their environment than the core level Cl 2p.

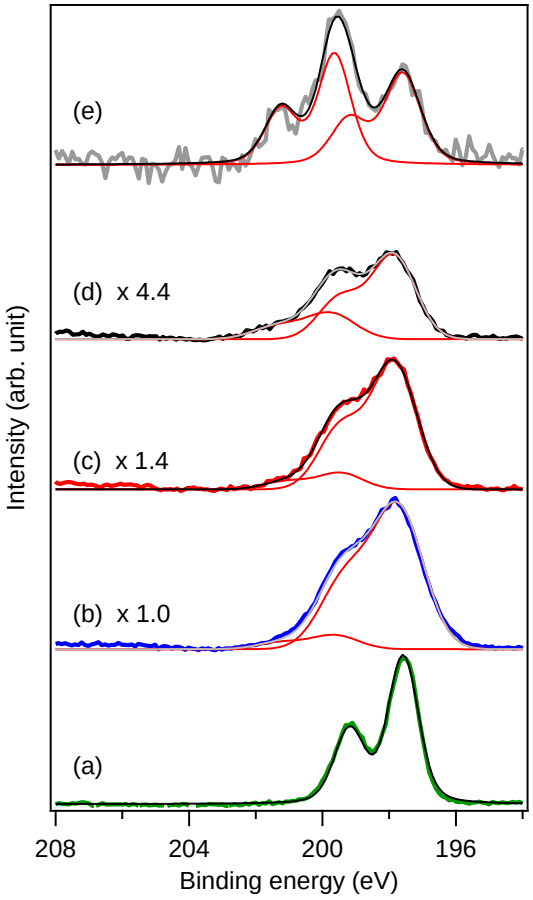

Figure 4. Cl 2p XPS spectra of MgAl-Cl-LDH [(a) *RH* = 0.000 (UHV, *hv* = 1487 eV, 293 K), (b) *RH* = 0.004 (0.1 mbar water, 293 K, *hv* = 1100 eV), (c) *RH* = 0.044 (1 mbar water, 293 K, *hv* = 1100 eV)] and Mg-Cl solution [4.5 mbar water, 274 K, (d) *hv* = 1100 eV, (e) *hv* = 420 eV]. Spectra intensities were normalized to insure proper readability: relative normalization factors are given in the graph for spectra recorded with *hv* = 1100 eV.

4) Mg-Cl solution

The surface of MgAl-Cl-LDH was probed by NAP-XPS with increasing relative humidity up to water droplets formation at the sample surface (at ~1°C and *RH* = 0.7, see Supporting Information section S2). The corresponding spectrum recorded in the 0-100 eV binding energy range presents O 2s (~24 eV), Mg 2p (~50 eV) and Mg 2s (~89 eV) peaks while Al 2p (~75 eV) component vanishes (see Figure 3). Moreover, the A_{O2s}/A_{Mg2p} ratio increases by a factor close to 7 with respect to dry MgAl-Cl-LDH. As the atomic O/Mg ratio equal 3 for dry MgAl-Cl-LDH, an O/Mg atomic ratio of 21 can be deduced in water droplets. Obviously, the increase of the O 2s component comes from liquid water. O 1s spectra (see Figure 5) support this attribution: the spectrum recorded under UHV presents only one component located at 531.9 eV corresponding to hydroxide moieties, while at *RH* = 0.7, the O 1s peak is centered at 532.8 eV corresponding to liquid water (see SI, see section S3).[3] Finally, Cl 2p spectrum (Figure 4) confirms the presence of Cl atoms. An atomic Cl/Mg ratio of 0.8 was estimated from Cl 2p and Mg 2p feature areas taking into accounts the attenuation of the photoelectrons by the gas phase following a procedure similar to the one described in SI (see section S3). All these results indicate that a water film containing both Mg and Cl species was detected in high humidity conditions. For the sake of simplicity, this film is labelled “Mg-Cl solution” in the following. Mechanisms leading to the formation of this film are discussed in the next section.

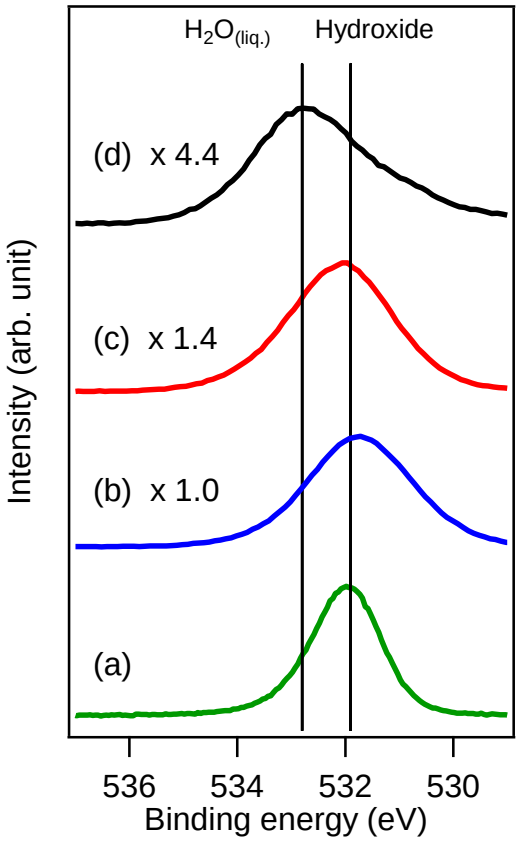

Figure 5. O 1s XPS spectra of MgAl-Cl-LDH [(a) *RH* = 0.000 (UHV, *hv* = 1487 eV, 293 K), (b) *RH* = 0.004 (0.1 mbar water, 293 K, *hv* = 1100 eV), (c) *RH* = 0.044 (1 mbar water, 293 K, *hv* = 1100 eV)] and (d) Mg-Cl solution (4.5 mbar water, 274 K, *hv* = 1100 eV). Spectra intensities were normalized to insure proper readability: relative normalization factors are given in the graph for spectra recorded with *hv* = 1100 eV.

Finally, a particular attention was paid to the Cl 2p signal of the Mg-Cl solution. The Cl 2p photoemission spectrum (*hv* = 1100 eV) can be properly fitted with two spin-orbit splitting doublets, with Cl $2p_{3/2}$ components located at 197.9 and 199.8 eV (see Figure 4 and Table 1). In these conditions, the 199.8 eV component represents 26 % of the signal area, following the trend observed at lower *RH*: the high binding energy component for spectra recorded at *RH* = 0.004 and 0.044 represents respectively 8 and 12% of the signal. However, it should be recalled that for *RH*

= 0.004 and 0.044, this high binding energy component could be an artifact due to badly compensated charge effect. Measurements performed on Mg-Cl solution make it possible to rule out this possibility. Actually, when Cl 2p photoemission spectrum was recorded with $h\nu$ = 420 eV the *FWHM* drops down to 1.3 eV for both components (which supports the absence of differential charging), confirming that the high binding energy component is not an artefact. A high binding energy component (shifted by ~2 eV with respect to Cl^-) was reported for a NaCl brine.[4] It should be attributed to an oxidized chlorine specie (additional results sustaining that conclusion are given in Supporting Information, see section S1 and S4), even if this oxidized specie is not necessarily the same than the one observed at low *RH* in solid LDH.

Discussion

Mg-Cl solution

At *RH* = 0.7, NAP-XPS showed the formation of an Mg-Cl solution on top of LDH surface. A complete description of the mechanism leading to the formation of such a layer is far beyond the scope of our study. Here, we will limit ourselves to point out conditions of concentration and *pH* that are consistent with this observation.

In acidic conditions, the full dissolution of MgAl-Cl-LDH leads to the total release of Mg^{2+} and Al^{3+} cations. Neutral or moderate alkaline conditions (1 g_{LDH} L^{-1}) result in incongruent dissolution of Mg^{2+} ([Mg^{2+}] in the range of 10^{-4} mol L^{-1}) exclusively.[34,35] In the latter case, an $Al(OH)_3$ layer forms at the Mg depleted surface of the solid.[34] This scheme is consistent with our observations at high *RH*: the NAP-XPS signal originates from an Mg containing layer essentially free of Al, while the layer screens any signal from the underneath solid. Interestingly, the Mg content of one LDH sheet is equal to the Mg content of a 6 nm thick film with O:Mg:Cl equal to 21:1:0.8. As the elastic mean free path of Al 2p photoelectron (*hv* = 1100 eV) is 2.5 nm (according to [36]), the dissolution of the first LDH sheet and the subsequent formation of a 6 nm film would be sufficient to screen any Al signal. Nevertheless, the Mg and Cl concentrations observed at *RH* = 0.7 are much higher (O/Mg = 21) than what is it observed in water excess condition[34,35] (O/Mg ~10^5). The phase diagram of the MgO-$MgCl_2$-H_2O ternary system[37,38] (at 296 K) may help to understand this difference: the composition of the system probed by NAP-XPS (O:Mg:Cl = 21:1:0.8) corresponds to a weight ratio MgO:$MgCl_2$:H_2O equal to 6:9:86. In this region of the ternary diagram, solid $Mg(OH)_2$ and $MgCl_2$ solution (free *pH* = 7.5) coexist at thermodynamic equilibrium. One should note that a metastable gel phase was also reported in that region:[37,38] it is commonly admitted that

reactive species (polynuclear Mg complexes) combine with the Cl^- and H_2O to form an amorphous hydrogel in which reduced diffusion rate prevents solid crystallisation.[39]

The following consistent scheme can be drawn. In a neutral/alkaline solution (water in excess), the MgAl-Cl-LDH surface is in dynamic equilibrium with Mg^{2+} solution (even containing Al species at high *pH*).[34,35,40] Under moderate *RH*, MgAl-Cl-LDH exchanges water with the surrounding gas phase, as evidenced by volumetric water adsorption measurements. At high *RH*, a Mg-Cl layer ($Mg(OH)_2$ saturated solution or metastable gel of the MgO-$MgCl_2$-H_2O system) forms on MgAl-Cl-LDH. The mechanism that would limit the complete deliquescence of the LDH remains unclear but one can infer that aluminum hydroxide whose formation on LDH results from the solubilization of magnesium ions may passivate the LDH surface that hinders further Mg^{2+} leaching.[34]

Finally, the question is: what would append for decreasing *RH* from high value (0.7 or higher) to low or null value. Actually, this is the well-known situation of drying the solubilized reaction product, which leads to the formation of solid LDH. Our interpretation of the experimental observations considers that Mg and Al oxychloride are able to form various phases at the LDH surface in contrast with numerous reports on LDH synthesis. The MgO-$MgCl_2$-H_2O phase diagram dispels this apparent inconsistency. Urwongse et Sorrel[37] report that the pH of an $Mg(OH)_2$ saturated solution (in the MgO-$MgCl_2$-H_2O system) decreases of few units for increasing concentration of $MgCl_2$ in the liquid phase, *i.e.* for decreasing *RH*. On the LDH surface, the hydrolysis of the aluminum hydroxides (resulting from the Mg depletion of the top sheet) would balance such an acidification and, in turn, could promote the reconstruction of the double hydroxide sheet. The molecular mechanisms leading to the formation of solid within the MgO-

$MgCl_2$-H_2O ternary system were reported,[41] but further efforts are needed to better understand how Al^{3+} (and other trivalent cations) alter these mechanisms and promote LDH formation.

To the best of our knowledge, this is the first description of the external surface of LDH at high *RH* and it may help the understanding of the behavior of this class of material under environmental conditions. Especially, the NAP-XPS shed light on the mechanism involving LDH surface properties for pollutants sequestration[10,11] or antibacterial effect.[12]

Chloride oxidation

As already reported, in previous studies[3,4,42] focusing on 6 M NaCl solution, two Cl 2p components of comparable intensities (in surface sensitive conditions) were observed at 197.6 and 199.8 eV. These components were ascribed to chloride in bulk water with a symmetric solvation shell (the low binding energy component) and to chloride at the gas/solution interface with an asymmetric solvation shell (the high binding energy component). The possibility of attributing the high binding energy component to ClO_x^- anions was also mentioned in [4], but was not explored at that time in sufficient depth.

In contrast to NaCl brines, for all studied conditions (*RH* = 0.000, 0.004 or 0.044 for MgAl-Cl-LDH as well as for Mg-Cl solution), the Cl 2p feature is largely dominated by one doublet located at 197.7 ± 0.2 eV (see Table 1). Thus, water radiolysis-induced changes in the chemistry of Cl^- is rather limited for RH ≤ 0.044, as the high binding energy component gives only a rather weak contribution to the total spectral weight (< 12 %). Second, no (significant) chemical shift can be detected for the chloride ion, within the explored RH range and hydration state: the binding energy of Cl^- remains close to that attributed to same ion in a symmetric water solvation shell.[3,4,42] Actually, we know that the solvation shell is essentially asymmetric in LDH interlayer due to confinement effects. Therefore, in the present case, because of the nearly constant Cl $2p_{3/2}$ binding energy (within the error bar) of the Cl^- component, NAP-XPS cannot distinguish hydrated from anhydrous chloride. The Cl 2p binding energy of the Cl^- ion is not sensitive to strong changes in its solvation shell as the LDH hydration increases. In retrospect, the attribution of the 199.8 eV component to chlorine species with an oxidation state greater than -I is reinvigorated. Different radiolytic mechanisms leading to oxidized chlorine in hydrated LDH or in solution are described

in the literature. In the following, the origin of oxidized chlorine species is discussed, embracing both the case of hydrated solid LDH and the case the Mg-Cl solution.

Chloride oxidation in MgAl-Cl-LDH

Considering radiolytic processes into hydrated LDH, Lainé *et al.*[13] suggested that the interaction of radiation with hydrated LDH produces an electron-hole pair (R1).

$$LDH \xrightarrow{\text{ionizing radiation}} e^- + h^+ \qquad (R1)$$

The hole can react with the water in the interlayer space producing $HO^\bullet$ and, then ClO^- according to:

$$h^+ + H_2O \rightarrow H^+ + HO^\bullet \qquad (R2)$$

$$HO^\bullet + Cl^- \rightarrow HOCl^{\bullet-} \qquad (R3)$$

$$2\ HOCl^{\bullet-} \rightarrow 2\ ClO^- + H_2 \qquad (R4)$$

This radiolytic mechanisms involving the creation of electron-hole pairs in the oxide and leading to the formation of ClO^- accounts for the 199.6 eV component observed for hydrated LDH.

Chloride oxidation in Mg-Cl solution

The Cl 2p spectra of the Mg-Cl solution are fitted with two Cl 2p doublets, corresponding to Cl atoms in two different chemical environments. A binding energy shift of 1.9 eV is found between the two Cl $2p_{3/2}$ peak positions. The comparison with liquid jet XPS experiments that are immune to radiolysis effects affecting the Cl^- ions (see for instance the KCl solution Cl 2p spectra published in the Supporting Information of [43]), rather pleads in favor of the formation of a chlorine atom with an oxidation state greater than -I (that of Cl^-). The ionization of aqueous solutions by highly

energetic photons leads to the decomposition of the water molecule and results in the ultrafast formation of radicals ($HO^{\bullet}$) together with the solvated electron. The direct ionization of chloride ion leads to $Cl^{\bullet}$ radical. All these reactive species contribute to oxidize chlorine in chloride solution and $Cl_2^{\bullet-}$, Cl_3^- or $HClO^{\bullet-}$ species were considered. [16,17]

In fact Cl_3^- is not stable at pH=7, and we do not believe it can be observed[44]. So, we have to look for a better candidate. A Cl $2p_{3/2}$ binding energy difference of 2.4 eV[45] between ClO^- and Cl^- in an aqueous solution with mixed NaCl and NaClO was determined by Winter *et al.*[45] using liquid microjet XPS. This binding energy shift is close to that found in this study (1.9 eV). Moreover, HClO, the conjugate acid of the hypochlorite ion (pKa = 7.5), can be also considered. Then, attribution of the 199.9 eV component is not completely clear but HClO and ClO^- species appear as trustworthy candidates. Note that pulse radiolysis studies[16,17] carried out in the nanosecond timescale did not point out the formation of ClO^-. Therefore, this species may be formed on considerably longer timescales.

Conclusions

To assess the behavior of LDHs materials with regard to water uptake, $[Mg_2Al(OH)_6]^+[Cl^-, y\ H_2O]$ was synthesis and characterized using water adsorption volumetry, XRD, FTIR and NAP-XPS spectroscopies. From vacuum to ambient condition, this material exhibits a limited swelling (the interlayer spacing increases from 7.44 Å to 7.69 Å) that can be fairly reproduced by DFT simulation considering one water molecule per chloride ion. FTIR measurements also provide insight into water/hydroxyl interactions that affect hydroxyl binding modes, while octahedral vibration mode remains essentially unchanged.

As far as we know, this work reports for the first time NAP-XPS measurements on LDH material under water pressure. The analysis of the O 2s and Mg 2p features makes it possible to quantify water uptake into the interlayer space for increasing pressure. The relevance of this method is supported by comparison with volumetric adsorption results. The shape of the valence band significantly evolves upon increasing *RH* as the average number of water molecules around the Cl^- ion increases. The O 2p feature is strengthened by water contribution, while the shift of the Cl 3p feature to higher binding energy (and its broadening) may reflect the stabilization of the outer shell through H-bonds formation. In contrast, the Cl 2p component of chloride ions (~197.6 eV) are poorly affected upon hydration. However, a new component at higher binding energy (~199.8 eV) appears. Its relative intensity increases with the increasing *RH*/number of water molecules around one Cl^-. We attribute it to ClO^- which appears due to complex radiolytic mechanisms involving electron-hole pair creation in the wet layered oxide.

The first description of the external surface of LDH at high *RH* was given. At *RH* = 0.7, the MgAl-Cl-LDH surface is Al free and presents hydrated Mg and Cl species. NAP-XPS shed light on the substantial exchange of divalent cations between LDH crystals and its hydration layer (O:Mg equal 21). That observation is relevant for the understanding of the mechanisms of LDH dissolution/formation and could be beneficial to optimize LHD for pollutant sequestration or antibacterial application (in particular when antibacterial mechanism involved bacterial/LDH contact).

In Mg-Cl solution we also report the growth of a component at a higher binding energy than that of Cl^-. The chemical shift is similar to what is observed in the case of the hydrated, but still solid LDH. This component in solution is also attributed to oxidized species of Cl^-. The two species may not be the same owing to the radiolytic phenomena that are different in the liquid and in the wet layered oxide, but we cannot help but note that their Cl 2p binding energies are very close. Extended radiolysis studies in solutions containing halogenide species consider $Cl_2^{\bullet-}$, Cl_3^- or $ClOH^{\bullet-}$. The formation of ClO^- and/or HClO is very likely.

Beyond the determination of the electronic structure of hydrated LDH, these results warn about radiolytic effects during NAP-XPS experiments. For further studies of materials in environmental conditions, soft X-ray irradiation will have to be carefully adjusted to avoid sample alteration. On the other hand, NAP-XPS appear as a new tool for *in operando* radiolysis investigations. In this framework, NAP-XPS should be able to provide chemical composition of hydrated system and its evolution under X-ray irradiation at a time resolution of ~1 s. This technique would be beneficial to anticipate the behavior and fate of materials designed for radionucleotide sequestration.

Supporting Information

Optical image of the probed sample; C 1s spectra; C, O and Cl content of contamination; Cl(+I) species in Mg-Cl solution: evolution under drying condition

Table 1. NAP-XPS binding energy values for Cl 2p level

	RH	Photon energy (eV)	Cl $2p_{3/2}$ (eV)	*FWHM* (eV)	%	Cl $2p_{3/2}$ (eV)	*FWHM* (eV)	%
MgAl-Cl-LDH @293 K	UHV	1487	197.6	1.1	100	-	-	-
	0.004	1100	197.7	1.8	92	199.6	1.6	8
	0.044	1100	197.8	1.6	88	199.5	1.6	12
Mg-Cl solution @274 K	0.7	1100	197.9	1.5	74	199.8	1.7	26
	0.7	420	197.6	1.3	48	199.6	1.2	52

AUTHOR INFORMATION

Corresponding Author

*romain.coustel@univ-lorraine.fr

ACKNOWLEDGMENT

We thank the PMD2X X-ray diffraction facility and Pierrick Durand of the laboratory Cristallographie, Résonance Magnétique et Modélisations, Université de Lorraine, for X-ray diffraction measurements (http://crm2.univ-lorraine.fr/lab/fr/services/pmd2x). XPS measurements were performed under UHV by A. Renard (LCPME-Nancy). Both XPS (UHV) and FTIR spectrometric measurements were performed at the spectroscopy and microscopy service facility of SMI LCPME (Université de Lorraine-CNRS– http://www.lcpme.cnrs-nancy.fr). The DFT calculations were possible thanks to high Performance Computing resources provided by the EXPLOR center hosted by the Université de Lorraine.

Anthony Boucly thanks Région Ile de France for his PhD grant HORS DIM EAU. The NAP-XPS experiment, managed by the LCPMR team (Sorbonne Université), was funded by the Ile-de-France Region (Photoémission Environnementale en Ile-de-France, SESAME n°090003524), by the Agence Nationale de la Recherche (Surfaces under Ambient Pressure with Electron Spectroscopies, ANR- 08-BLAN-0096), and by Université Pierre et Marie Curie (now Sorbonne Université). Synchrotron SOLEIL supported the integration of the setup to TEMPO beamline. The authors thank warmly the TEMPO beamline staff (Dr Fausto Sirotti and Dr Mathieu Silly) for their efficient assistance.

REFERENCES

(1) Zhong, L.; Chen, D.; Zafeiratos, S. A Mini Review of in Situ Near-Ambient Pressure XPS Studies on Non-Noble, Late Transition Metal Catalysts. *Catal. Sci. Technol.* **2019**, *9* (15), 3851–3867. https://doi.org/10.1039/C9CY00632J.

(2) Liu, H.; Zakhtser, A.; Naitabdi, A.; Rochet, F.; Bournel, F.; Salzemann, C.; Petit, C.; Gallet, J.-J.; Jie, W. Operando Near-Ambient Pressure X-Ray Photoelectron Spectroscopy Study of the CO Oxidation Reaction on the Oxide/Metal Model Catalyst ZnO/Pt(111). *ACS Catal.* **2019**, *9* (11), 10212–10225. https://doi.org/10.1021/acscatal.9b02883.

(3) Tissot, H.; Gallet, J.-J.; Bournel, F.; Olivieri, G.; Silly, M. G.; Sirotti, F.; Boucly, A.; Rochet, F. The Electronic Structure of Saturated NaCl and NaI Solutions in Contact with a Gold Substrate. *Top. Catal.* **2016**, *59* (5–7), 605–620. https://doi.org/10.1007/s11244-015-0530-6.

(4) Tissot, H.; Olivieri, G.; Gallet, J.-J.; Bournel, F.; Silly, M. G.; Sirotti, F.; Rochet, F. Cation Depth-Distribution at Alkali Halide Aqueous Solution Surfaces. *J. Phys. Chem. C* **2015**, *119* (17), 9253–9259. https://doi.org/10.1021/jp512695c.

(5) Boucly, A.; Rochet, F.; Arnoux, Q.; Gallet, J.-J.; Bournel, F.; Tissot, H.; Marry, V.; Dubois, E.; Michot, L. Soft X-Ray Heterogeneous Radiolysis of Pyridine in the Presence of Hydrated Strontium-Hydroxyhectorite and Its Monitoring by Near-Ambient Pressure Photoelectron Spectroscopy. *Sci. Rep.* **2018**, *8* (1), 6164. https://doi.org/10.1038/s41598-018-24329-8.

(6) Liu, Y.; Gao, Y.; Wang, Q.; Lin, W. The Synergistic Effect of Layered Double Hydroxides with Other Flame Retardant Additives for Polymer Nanocomposites: A Critical Review. *Dalton Trans.* **2018**, *47* (42), 14827–14840. https://doi.org/10.1039/C8DT02949K.

(7) Yang, Z.; Zhang, C.; Zeng, G.; Tan, X.; Wang, H.; Huang, D.; Yang, K.; Wei, J.; Ma, C.; Nie, K. Design and Engineering of Layered Double Hydroxide Based Catalysts for Water Depollution by Advanced Oxidation Processes: A Review. *J. Mater. Chem. A* **2020**, *8* (8), 4141–4173. https://doi.org/10.1039/C9TA13522G.

(8) Fahel, J.; Kim, S.; Durand, P.; André, E.; Carteret, C. Enhanced Catalytic Oxidation Ability of Ternary Layered Double Hydroxides for Organic Pollutants Degradation. *Dalton Trans.* **2016**, *45* (19), 8224–8235. https://doi.org/10.1039/C6DT00441E.

(9) Ameena Shirin, V. K.; Sankar, R.; Johnson, A. P.; Gangadharappa, H. V.; Pramod, K. Advanced Drug Delivery Applications of Layered Double Hydroxide. *J. Controlled Release* **2021**, *330*, 398–426. https://doi.org/10.1016/j.jconrel.2020.12.041.

(10) Di Bitetto, A.; Kervern, G.; André, E.; Durand, P.; Carteret, C. Carbonate–Hydrogenocarbonate Coexistence and Dynamics in Layered Double Hydroxides. *J. Phys. Chem. C* **2017**, *121* (11), 6104–6112. https://doi.org/10.1021/acs.jpcc.6b12192.

(11) Wang, L.; Li, Z.; Wu, Q.; Huang, Z.; Yuan, L.; Chai, Z.; Shi, W. Layered Structure-Based Materials: Challenges and Opportunities for Radionuclide Sequestration. *Environ. Sci. Nano* **2020**, *7* (3), 724–752. https://doi.org/10.1039/C9EN01429B.

(12) Awassa, J.; Soulé, S.; Cornu, D.; Ruby, C.; El-Kirat-Chatel, S. Understanding the Role of Surface Interactions in the Antibacterial Activity of Layered Double Hydroxide Nanoparticles by Atomic Force Microscopy. *Nanoscale* **2022**, *14* (29), 10335–10348. https://doi.org/10.1039/D2NR02395D.

(13) Lainé, M.; Liao, Y.; Varenne, F.; Picot, P.; Michot, L. J.; Barruet, E.; Geertsen, V.; Thill, A.; Pelletier, M.; Brubach, J.-B.; Roy, P.; Le Caër, S. Tuning the Nature of the Anion in

Hydrated Layered Double Hydroxides for H_2 Production under Ionizing Radiation. *ACS Appl. Nano Mater.* **2018**, *1* (9), 5246–5257. https://doi.org/10.1021/acsanm.8b01240.
(14) Manohara, G. V.; Kunz, D. A.; Kamath, P. V.; Milius, W.; Breu, J. Homogeneous Precipitation by Formamide Hydrolysis: Synthesis, Reversible Hydration, and Aqueous Exfoliation of the Layered Double Hydroxide (LDH) of Ni and Al. *Langmuir* **2010**, *26* (19), 15586–15591. https://doi.org/10.1021/la103108f.
(15) Komulainen, S.; Pursiainen, J.; Perämäki, P.; Lajunen, M. Complexation of Fe(III) with Water-Soluble Oxidized Starch. *Starch - Stärke* **2013**, *65* (3–4), 338–345. https://doi.org/10.1002/star.201200127.
(16) El Omar, A. K.; Schmidhammer, U.; Rousseau, B.; LaVerne, J.; Mostafavi, M. Competition Reactions of $H_2O^{\bullet+}$ Radical in Concentrated Cl^- Aqueous Solutions: Picosecond Pulse Radiolysis Study. *J. Phys. Chem. A* **2012**, *116* (47), 11509–11518. https://doi.org/10.1021/jp309381z.
(17) Balcerzyk, A.; Schmidhammer, U.; El Omar, A. K.; Jeunesse, P.; Larbre, J.-P.; Mostafavi, M. Picosecond Pulse Radiolysis of Direct and Indirect Radiolytic Effects in Highly Concentrated Halide Aqueous Solutions. *J. Phys. Chem. A* **2011**, *115* (33), 9151–9159. https://doi.org/10.1021/jp203609e.
(18) Le Caër, S. Water Radiolysis: Influence of Oxide Surfaces on H2 Production under Ionizing Radiation. *Water* **2011**, *3* (1), 235–253. https://doi.org/10.3390/w3010235.
(19) Di Bitetto, A.; André, E.; Carteret, C.; Durand, P.; Kervern, G. Probing the Dynamics of Layered Double Hydroxides by Solid-State ^{27}Al NMR Spectroscopy. *J. Phys. Chem. C* **2017**, *121* (13), 7276–7281. https://doi.org/10.1021/acs.jpcc.6b13106.
(20) Iyi, N.; Yamada, H.; Sasaki, T. Deintercalation of Carbonate Ions from Carbonate-Type Layered Double Hydroxides (LDHs) Using Acid–Alcohol Mixed Solutions. *Appl. Clay Sci.* **2011**, *54* (2), 132–137. https://doi.org/10.1016/j.clay.2011.07.017.
(21) Polack, F.; Silly, M.; Chauvet, C.; Lagarde, B.; Bergeard, N.; Izquierdo, M.; Chubar, O.; Krizmancic, D.; Ribbens, M.; Duval, J.-P.; Basset, C.; Kubsky, S.; Sirotti, F.; Garrett, R.; Gentle, I.; Nugent, K.; Wilkins, S. TEMPO: A New Insertion Device Beamline at SOLEIL for Time Resolved Photoelectron Spectroscopy Experiments on Solids and Interfaces; Melbourne (Australia), 2010; pp 185–188. https://doi.org/10.1063/1.3463169.
(22) Dovesi, R.; Orlando, R.; Civalleri, B.; Roetti, C.; Saunders, V. R.; Zicovich-Wilson, C. M. CRYSTAL: A Computational Tool for the *Ab Initio* Study of the Electronic Properties of Crystals. *Z. Für Krist. - Cryst. Mater.* **2005**, *220* (5–6), 571–573. https://doi.org/10.1524/zkri.220.5.571.65065.
(23) Dovesi, R.; Orlando, R.; Erba, A.; Zicovich-Wilson, C. M.; Civalleri, B.; Casassa, S.; Maschio, L.; Ferrabone, M.; De La Pierre, M.; D'Arco, P.; Noël, Y.; Causà, M.; Rérat, M.; Kirtman, B. CRYSTAL14: A Program for the Ab Initio Investigation of Crystalline Solids. *Int. J. Quantum Chem.* **2014**, *114* (19), 1287–1317. https://doi.org/10.1002/qua.24658.
(24) Andre, E.; Fahel, J.; Carteret, C. Modelling the Structure and Vibrational Properties of Layered Double Hydroxides. In *Energy Technology 2015*; Jha, A., Wang, C., Neelameggham, N. R., Guillen, D. P., Li, L., Belt, C. K., Kirchain, R., Spangenberger, J. S., Johnson, F., Gomes, A. J., Pandey, A., Hosemann, P., Eds.; Springer International Publishing: Cham, 2015; pp 317–323. https://doi.org/10.1007/978-3-319-48220-0_35.
(25) Costa, D. G.; Rocha, A. B.; Diniz, R.; Souza, W. F.; Chiaro, S. S. X.; Leitão, A. A. Structural Model Proposition and Thermodynamic and Vibrational Analysis of

Hydrotalcite-Like Compounds by DFT Calculations. *J. Phys. Chem. C* **2010**, *114* (33), 14133–14140. https://doi.org/10.1021/jp1033646.
(26) Costa, D. G.; Rocha, A. B.; Souza, W. F.; Chiaro, S. S. X.; Leitão, A. A. Ab Initio Simulation of Changes in Geometry, Electronic Structure, and Gibbs Free Energy Caused by Dehydration of Hydrotalcites Containing Cl^- and CO_3^{2-} Counteranions. *J. Phys. Chem. B* **2011**, *115* (13), 3531–3537. https://doi.org/10.1021/jp110668s.
(27) Jayanthi, K.; Nagendran, S.; Kamath, P. V. Layered Double Hydroxides: Proposal of a One-Layer Cation-Ordered Structure Model of Monoclinic Symmetry. *Inorg. Chem.* **2015**, *54* (17), 8388–8395. https://doi.org/10.1021/acs.inorgchem.5b01050.
(28) Lee, C.; Yang, W.; Parr, R. G. Development of the Colle-Salvetti Correlation-Energy Formula into a Functional of the Electron Density. *Phys. Rev. B* **1988**, *37* (2), 785–789. https://doi.org/10.1103/PhysRevB.37.785.
(29) Becke, A. D. Density-Functional Thermochemistry. III. The Role of Exact Exchange. *J. Chem. Phys.* **1993**, *98* (7), 5648–5652. https://doi.org/10.1063/1.464913.
(30) Grimme, S. Accurate Description of van Der Waals Complexes by Density Functional Theory Including Empirical Corrections. *J. Comput. Chem.* **2004**, *25* (12), 1463–1473. https://doi.org/10.1002/jcc.20078.
(31) Grimme, S. Semiempirical GGA-Type Density Functional Constructed with a Long-Range Dispersion Correction. *J. Comput. Chem.* **2006**, *27* (15), 1787–1799. https://doi.org/10.1002/jcc.20495.
(32) Iyi, N.; Fujii, K.; Okamoto, K.; Sasaki, T. Factors Influencing the Hydration of Layered Double Hydroxides (LDHs) and the Appearance of an Intermediate Second Staging Phase. *Appl. Clay Sci.* **2007**, *35* (3–4), 218–227. https://doi.org/10.1016/j.clay.2006.08.011.
(33) Richardson, M. C.; Braterman, P. S. Infrared Spectra of Oriented and Nonoriented Layered Double Hydroxides in the Range from 4000 to 250 Cm^{-1} , with Evidence for Regular Short-Range Order in a Synthetic Magnesium−Aluminum LDH with Mg:Al = 2:1 but Not with Mg:Al = 3:1. *J. Phys. Chem. C* **2007**, *111* (11), 4209–4215. https://doi.org/10.1021/jp064744w.
(34) Jobbágy, M.; Regazzoni, A. E. Dissolution of Nano-Size Mg–Al–Cl Hydrotalcite in Aqueous Media. *Appl. Clay Sci.* **2011**, *51* (3), 366–369. https://doi.org/10.1016/j.clay.2010.11.027.
(35) Boclair, J. W.; Braterman, P. S. Layered Double Hydroxide Stability. 1. Relative Stabilities of Layered Double Hydroxides and Their Simple Counterparts. *Chem. Mater.* **1999**, *11* (2), 298–302. https://doi.org/10.1021/cm980523u.
(36) Seah, M. P. An Accurate and Simple Universal Curve for the Energy-Dependent Electron Inelastic Mean Free Path: Simple, Accurate, Universal Expression for IMFPs. *Surf. Interface Anal.* **2012**, *44* (4), 497–503. https://doi.org/10.1002/sia.4816.
(37) Urwongse, L.; Sorrell, C. A. The System MgO-MgCl2-H2O at 23oC. *J. Am. Ceram. Soc.* **1980**, *63* (9–10), 501–504. https://doi.org/10.1111/j.1151-2916.1980.tb10752.x.
(38) Sorrell, C. A.; Armstrong, C. R. Reactions and Equi Ibria in Magnesium Oxych Oride Cements. *J. Am. Ceram. Soc.* **1976**, *59* (1–2), 51–54. https://doi.org/10.1111/j.1151-2916.1976.tb09387.x.
(39) Jin, F. Magnesium Oxychloride Cement. In *Magnesia Cements*; Elsevier, 2020; pp 29–74. https://doi.org/10.1016/B978-0-12-391925-0.00009-1.
(40) Johnson, C. A.; Glasser, F. P. Hydrotalcite-like Minerals (M2Al(OH)6(CO3)0.5.XH2O, Where M = Mg, Zn, Co, Ni) in the Environment; Synthesis, Characterization and

Thermodynamic Stability. *Clays Clay Miner.* **2003**, *51* (1), 1–8. https://doi.org/10.1346/CCMN.2003.510101.
(41) Dehua, D.; Chuanmei, Z. The Formation Mechanism of the Hydrate Phases in Magnesium Oxychloride Cement11This Paper Was Originally Submitted to Advanced Cement Based Materials. It Was Received at the Editorial Office of Cement and Concrete Research on 20 August 1998 and Accepted in Final Form on 16 December 1998. *Cem. Concr. Res.* **1999**, *29* (9), 1365–1371. https://doi.org/10.1016/S0008-8846(98)00247-6.
(42) Cheng, M. H.; Callahan, K. M.; Margarella, A. M.; Tobias, D. J.; Hemminger, J. C.; Bluhm, H.; Krisch, M. J. Ambient Pressure X-Ray Photoelectron Spectroscopy and Molecular Dynamics Simulation Studies of Liquid/Vapor Interfaces of Aqueous NaCl, RbCl, and RbBr Solutions. *J. Phys. Chem. C* **2012**, *116* (7), 4545–4555. https://doi.org/10.1021/jp205500h.
(43) Pérez Ramírez, L.; Boucly, A.; Saudrais, F.; Bournel, F.; Gallet, J.-J.; Maisonhaute, E.; Milosavljević, A. R.; Nicolas, C.; Rochet, F. The Fermi Level as an Energy Reference in Liquid Jet X-Ray Photoelectron Spectroscopy Studies of Aqueous Solutions. *Phys. Chem. Chem. Phys.* **2021**, *23* (30), 16224–16233. https://doi.org/10.1039/D1CP01511G.
(44) Giordano, M. C.; Macagno, V. A.; Serano, L. E. Trichloride Ion Formation Constant in Acetonitrile Solutions. *Anal. Chem.* **1973**, *45* (1), 205–207. https://doi.org/10.1021/ac60323a026.
(45) Ottosson, N.; Vácha, R.; Aziz, E. F.; Pokapanich, W.; Eberhardt, W.; Svensson, S.; Öhrwall, G.; Jungwirth, P.; Björneholm, O.; Winter, B. Large Variations in the Propensity of Aqueous Oxychlorine Anions for the Solution/Vapor Interface. *J. Chem. Phys.* **2009**, *131* (12), 124706. https://doi.org/10.1063/1.3236805.

TOC Graphic

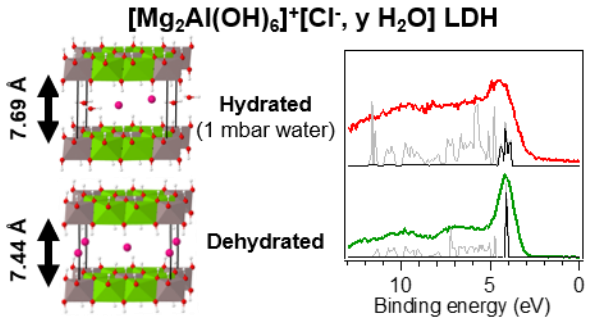
[Mg2Al(OH)6]+[Cl-, y H2O] LDH
7.69 Å
Hydrated
(1 mbar water)
7.44 Å
Dehydrated
10
5
0
Binding energy (eV)